JOURNAL OF GEOPHYSICAL RESEARCH: SOLID EARTH, VOL. 118, 748–758, doi:10.1002/jgrb.50093, 2013

The utility of atmospheric analyses for the mitigation of artifacts in InSAR

James Foster,[1] John Kealy,[1] Tiziana Cherubini,[1] Steven Businger,[1] Zhong Lu,[2] and Michael Murphy[3]

Received 11 June 2012; revised 8 January 2012; accepted 14 January 2012; published 26 February 2013.

[1] The numerical weather models (NWMs) developed by the meteorological community are able to provide accurate analyses of the current state of the atmosphere in addition to the predictions of the future state. To date, most attempts to apply the NWMs to estimate the refractivity of the atmosphere at the time of satellite synthetic aperture radar (SAR) data acquisitions have relied on predictive models. We test the hypothesis that performing a final assimilative routine, ingesting all available meteorological observations for the times of SAR acquisitions, and generating customized analyses of the atmosphere at those times will better mitigate atmospheric artifacts in differential interferograms. We find that, for our study area around Mount St. Helens (Amboy, Washington, USA), this approach is unable to model the refractive changes and provides no mean benefit for interferogram analysis. The performance is improved slightly by ingesting atmospheric delay estimates derived from the limited local GPS network; however, the addition of water vapor products from the GOES satellites reduces the quality of the corrections. We interpret our results to indicate that, even with this advanced approach, NWMs are not a reliable mitigation technique for regions such as Mount St. Helens with highly variable moisture fields and complex topography and atmospheric dynamics. It is possible, however, that the addition of more spatially dense meteorological data to constrain the analyses might significantly improve the performance of weather modeling of atmospheric artifacts in satellite radar interferograms.

Citation: Foster, J., J. Kealy, T. Cherubini, S. Businger, Z. Lu, and M. Murphy (2013), The utility of atmospheric analyses for the mitigation of artifacts in InSAR, *J. Geophys. Res. Solid Earth*, *118*, 748–758, doi:10.1002/jgrb.50093.

1. Introduction

[2] Although interferometric synthetic aperture radar (InSAR) studies have already yielded unprecedented high-resolution spatial coverage of earthquakes [e.g., *Massonnet et al.*, 1993; *Sandwell et al.*, 2000; *Fialko et al.*, 2001; *Jónsson et al.*, 2002], volcanoes [e.g., *Poland and Lu*, 2008], and fault hazard and creep processes [e.g., *Burgmann et al.*, 2000], the technique still has not realized its full potential for use when atmospheric water vapor conditions are not optimal during scene acquisition, especially when measuring discrete events. Evaluating the hazard presented by a volcano, for example, depends on recognizing quickly whether it is inflating or deflating. Other small amplitude, transient signals that might be generated, for example, by accelerating slip on a blind thrust fault underlying Los Angeles (which may be a precursor to a major earthquake [e.g., *Walls et al.*, 1998; *Shaw and Shearer*, 1999]), may also be obscured in InSAR images by noise generated by the atmosphere. A related issue derives from the common practice of refining orbital parameters for the SAR satellite when processing InSAR data. Orbital errors are manifested in interferograms as linear phase-ramps; however, long-wavelength weather patterns may induce similar features. The ambiguity between these two sources of artifacts could lead to inappropriate corrective steps in the processing on InSAR data, possibly masking real long-wavelength ground motion signals.

[3] Variations in refractivity of the atmosphere between the two times of SAR data acquisitions will change the travel time of the radar waves and hence the apparent range to the ground. This is indistinguishable from range changes due to actual ground motion [*Zebker et al.*, 1997; *Hanssen*, 1998; *Hanssen et al.*, 1999] and can mask or even reverse the sense of apparent deformation signals. Temperature and pressure variations change the refractivity, but the biggest impact is caused by changes in water vapor distribution. The difficulty in measuring or estimating these parameters with the accuracy and spatial density required to improve InSAR interferograms is one of the biggest factors limiting InSAR for operational hazard monitoring and some geodetic investigations.

All Supporting Information may be found in the online version of this article.

[1]School of Ocean and Earth Science and Technology, University of Hawaii, Honolulu, Hawaii, USA.
[2]Cascades Volcano Observatory, U.S. Geological Survey, Vancouver, Washington, USA.
[3]Monash University, Melbourne, Victoria, Australia.

Corresponding author: J. Foster, School of Ocean and Earth Science and Technology, University of Hawaii, 1680 East West Road, Honolulu, HI 96822, USA. (jfoster@ soest.hawaii.edu)

2169-9313/13/10.1002/jgrb.50093

[4] There are three categories of approach that are currently being used or explored for the mitigation of atmospheric artifacts in InSAR. The first is based on the InSAR processing itself and leverages the large data sets available for some locations. For example, traditional stacking estimates average ground motions over the entire time window covered by the SAR scenes. Although this approach improves the signal-to-noise ratio, it requires a correspondingly long time before a signal can be identified [*Emardson et al*., 2003], limiting its utility for rapid detection, analysis, and dissemination. It also restricts the analysis to long-term, relatively linear, deformation signals. More recent algorithmic developments allow for the formation of a time series of InSAR pixel displacements [*Ferretti et al*., 2001; *Berardino et al*., 2002; *Hooper et al*., 2004], isolating the atmospheric contribution by exploiting the expected temporal decorrelation of atmospheric delay perturbations. Once again, this requires a large number of scenes, and although it gives access to possible nonlinear and transient ground motions, it depends on the statistical assumptions imposed during the processing to separate the various components contributing to the total apparent displacements. Using only SAR data processing, it is generally difficult, or impossible, to quantitatively validate the parameters used and the residual phase screens produced.

[5] A second approach attempts to model the atmosphere in InSAR images based on concurrent observations [*Webley et al*., 2002], sometimes guided by numerical weather model (NWM) predictions [*Wadge et al*., 2002]. This approach has shown promise for times when, for example, relatively cloud-free conditions allowed the Medium-Resolution Imaging Spectrometer sensor onboard the Envisat satellite to acquire accurate maps of water vapor at the same time as the advanced SAR sensor collects SAR data [*Li et al*., 2005, 2006]. Work in southern California has found that delay estimates from the extremely dense and extensive GPS network around Los Angeles are able to generate atmospheric phase screens that reduce the noise in interferograms significantly [*Onn and Zebker*, 2006]. For most locations of interest, however, any ground-based network of instruments will offer poor spatial resolution, and space-based instruments are typically limited to cloud-free daylight hours or sparse repeat times.

[6] The third technique exploits the many years of development of extremely sophisticated NWMs by the meteorological community. Initial attempts to adapt these tools to InSAR mitigation used high-resolution custom weather models nested within coarser, global, weather models to estimate the atmospheric delay [*Webley et al*., 2004; *Foster et al*., 2006; *Puysségur et al*., 2007]. The predicted delays are used to generate a synthetic interferogram that is compared with the observed interferogram and/or subtracted from it. This should reduce the atmospheric noise, increasing the signal-to-noise ratio for InSAR over short temporal and spatial scales so that geodetic signals can be more reliably identified, modeled, and interpreted.

[7] A study using this approach for the Island of Hawaii [*Foster et al*., 2006] found that it showed promise; however, the research was constrained by having to use predictions on a 3-km (horizontal) grid that is too coarse for most InSAR purposes. Studies in other locations using a range of different NWM prediction packages have also shown promise but with somewhat equivocal success [e.g., *Webley et al*., 2004; *Puysségur et al*., 2007; *Eff-Darwich et al*., 2012], with the most encouraging results originating from continental locations with more predictable atmospheric conditions [*Elliott et al*., 2008; *Doin et al*., 2009; *Jolivet et al*., 2011; *Pinel et al*., 2011]. All these studies used predicted fields, in some cases for the specific time of the SAR data acquisition, whereas others interpolated between weather model output time slices. Weather prediction is notoriously difficult and sensitive to initial conditions, so it is not surprising that predicted delays often do not closely match many of the features observed in interferograms that are clearly atmospheric artifacts. Current SAR systems do not provide data in, or even generally near, real time so, for InSAR applications, the state of the atmosphere at the acquisition time does not need to be predicted to be ready for use as a correction term in an operational system: it simply needs to be modeled or analyzed [*Barnes*, 1964; *McGinley*, 1989] in as much detail as possible.

[8] Recognizing this, we have extended the standard approach of using predictions from weather models for SAR atmospheric mitigation and established a "hind-casting" system: we take weather model predictions of the atmospheric state—the end product for most previous mitigation approaches—and use them as the initial conditions for a further step that performs high-resolution meteorological analyses, incorporating all the additional meteorological information available for the time of the SAR acquisitions (Figure 1). We then use these analyses in the same manner as other investigators to produce line-of-sight atmospheric delay maps. We focus our study on Mount St. Helens (Figure 2), where the dome-building eruption from September 2004 to early 2008 provides us with a volcanic signal due to deflation of the subsurface magma reservoir, centered several kilometers below the crater [*Lisowski et al*., 2008]. The atmospheric setting of Mount St. Helens is broadly representative of a large number of other volcanoes. It is close enough to the ocean (~100 km) to be strongly influenced by the moist marine boundary layer and the interplay between it, the drier air from the interior, and the complex orography. Previous InSAR studies at Mount St. Helens have noted the impact of the atmosphere on interferograms, obscuring the small but important signal associated with changes in magma chamber pressure [*Poland and Lu*, 2008]. This volcano provides a demanding yet realistic test of the ability of our proposed approach to help distinguish between purely atmospheric artifacts, which will often be correlated in a complex way with elevation, and real volcanic signals, which may also be elevation correlated.

2. Atmospheric Analyses

[9] High-resolution mesoscale weather models, such as the MM5 (National Center for Atmospheric Research-Penn State Mesoscale Model Version 5) [*Grell et al*., 1995] and the WRF (Weather Research and Forecasting) [*Skamarock et al*., 2005], and analyses such as produced by Local Analysis and Prediction System (LAPS) *McGinley* [1989] and *McGinley et al*. [1991] are employed regularly in research and/or operational theaters by the academic, civilian, and military meteorological communities [*Businger et al*., 2001].

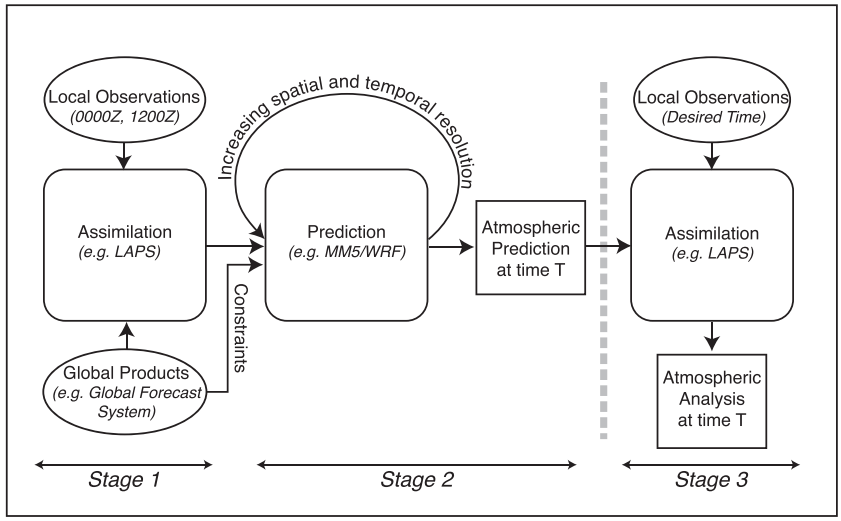

Figure 1. Schematic diagram illustrating our NWM processing approach. Previous efforts used the predictions from the end of Stage 2 (to the left of the heavy dashed gray line) for their correction fields. We introduce the additional Stage 3 (to the right of the heavy dashed gray line) with a final LAPS assimilation to produce a better-constrained, time-specific analysis.

2.1. MM5

[10] MM5 is a limited-area, nonhydrostatic, terrain-following sigma-coordinate model designed to simulate mesoscale and regional-scale atmospheric circulation [*Grell et al*., 1995]. MM5 predicts the thermodynamic properties of the atmosphere, including temperature, pressure, and moisture fields at selectable horizontal resolution. The vertical resolution of the MM5 field is density weighted with the greatest resolution (tens of meters) near the surface. The MM5 physics package uses the grid-resolvable Reisner-2 moisture scheme [*Reisner et al*., 1998] that includes graupel and ice condensation nuclei and allows coexistence of mixed water phases; the Kain–Fritsch cumulus convection scheme [*Kain and Fritsch*, 1990]; a high-resolution Medium-Range Forecast model boundary layer scheme [*Troen and Mahrt*, 1986]; and a longwave/shortwave radiation scheme that allows interaction with water vapor, clouds, precipitation, and the surface [*Stephens*, 1978; *Garand*, 1983].

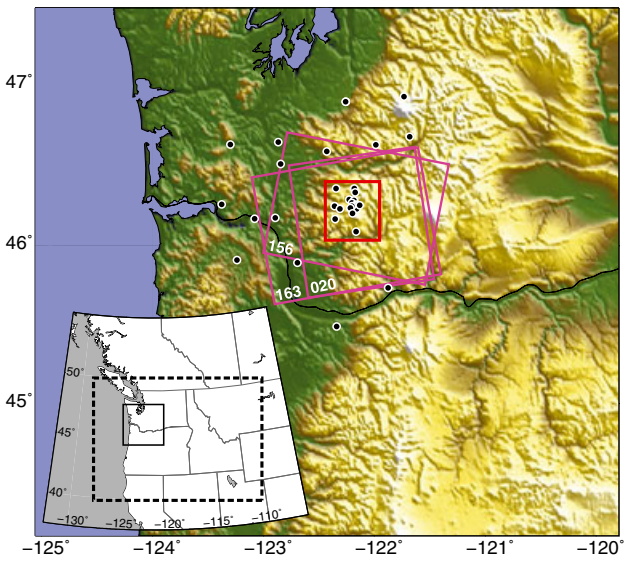

Figure 2. Domain for the 1-km LAPS with shaded topography, GPS sites (white-rimmed dots), footprints for the three different SAR data sets (purple boxes), and statistical analysis area centered on Mount St. Helens (red box). (inset) Extent of the MM5 4-km regional domain (dashed line) and the 1-km LAPS domain (solid line).

2.2. LAPS

[11] For operational high-resolution NWMs such as MM5, initial and boundary conditions for each run of the predictive model are provided by an analysis package. One such package, the LAPS, was developed at the NOAA Forecast System Laboratory to merge all the available data sources over the area of interest and produce coherent analyses of the atmosphere [*Hiemstra et al*., 2006]. LAPS first performs an analysis of the surface fields followed by a wind analysis, a temperature analysis, and finally a cloud-field analysis. All of the above make use of a first-guess field usually provided by a regional or global NWM. The LAPS wind analysis uses all available data sources in a two-pass objective analysis. Background model grids are used as a first-guess analysis from which observation residuals are calculated. The observation residuals are subject to quality-control checks.

[12] LAPS can integrate a wide variety of data types, from a variety of sources, including surface observing systems, Doppler radar, satellites, wind and temperature profilers, radiometric profilers, radiosonde profiles, buoy data, and GPS total precipitable water vapor determined from signal delay. Any new source of data can be incorporated easily as long as is provided in a recognized format (e.g., NetCDF file format) and the meteorological observations use recognized parameters (e.g., slant water vapor). Our LAPS approach is based on the operational system developed by the Mauna Kea Weather Center [*Cherubini et al*., 2006].

3. Ancillary Data

3.1. MADIS

[13] The Meteorological Assimilation Data Ingest System (MADIS) provides an integrated database containing real-time and archived (from real-time) observations from a large number of federal and state agencies, private companies, volunteers, and universities for use by the greater meteorological community. MADIS ingests data from its various sources, provides quality control, and makes the results available in a common format (http://madis.noaa.gov/). The MADIS data sets used for the region of our experiments include (i) surface networks, (ii) aircraft data, (iii) radiosonde data, and (iv) atmospheric motion vectors (satellite winds).

3.2. GOES

[14] For our application, with temporal resolution a priority, the GOES offers potentially valuable quasi-continuous observations (every 15 min) for the continental USA. LAPS reads the GOES visible and infrared channels and extracts information on water vapor and cloud cover [*Albers et al*., 1996].

3.3. GPS

[15] Data from the local and regional networks of permanent GPS stations were downloaded from the University NAVSTAR Consortium (UNAVCO) archives (ftp://data-out.unavco.org/pub/rinex) and processed, along with IGS sites from elsewhere in North America, using the GAMIT software [*Herring et al*., 2006] to generate half-hourly estimates of zenith delay [*Bevis et al*., 1992] used to provide atmospheric delay estimates for assimilation into the weather analysis. LAPS was originally written to use GPS data to provide absolute reference values to adjust the precipitable water maps generated by the GOES satellites. A minor update was needed to allow us to incorporate GPS delays into the analysis without accompanying GOES data.

4. Modeling Approach

[16] Figure 1 illustrates the processing flow for weather model-based InSAR mitigation and has the following stages:

[17] 1) Initial and boundary conditions are generated for a regional domain (e.g., by a package such as LAPS) typically by assimilating all regional meteorological observations for the model start time into a background global or regional analysis.

[18] 2) The NWM (e.g., MM5/WRF) is run in an iterative fashion, with nested domains providing increasing spatial and temporal resolution of the forecast for regions of specific interest.

[19] 3) The final, highest-resolution, prediction is used as the initial background for a further analysis that ingests all locally available meteorological data and assimilates them with the background predicted fields to produce a (possibly even higher resolution) analysis for that time.

[20] Stages 1 and 2 require a large amount of effort and experience to establish and operate effectively and accurately for any given area and are probably prohibitively difficult for most InSAR users to attempt. For many areas in the world, however, weather models are already in operation, so there is no need to try and duplicate that work. We leverage the operational weather prediction system being run by the University of Washington/Northwest Modeling Consortium. We use their MM5 model output, which includes of predictions of the temperature, pressure, and moisture fields, at a 4-km horizontal resolution for the Pacific Northwest. The output from Stage 2 provides the predicted fields that previous investigators have used to calculate the atmospheric refraction and attempt to mitigate its effect on the SAR data. We further develop and extended this approach by adding Stage 3. In Stage 3, we run LAPS on the output of the Stage 2 (Figure 1) along with additional meteorological data. We perform 3 separate LAPS analyses to investigate the impact of ingesting progressively more ancillary data. Each run uses the high-resolution topography data and the same MM5 prediction fields for background and then includes (1) all available local data from the MADIS meteorological data archive, (2) MADIS plus GPS-derived estimates of integrated water vapor (IWV), and (3) MADIS, GPS IWV, and GOES weather satellite cloud and water vapor fields. The LAPS analyses provided output fields on a 1-km horizontal grid for a smaller domain centered on Mount St. Helens. As with previous work, these grids are then converted into estimates of atmospheric refractivity, and ray tracing is used to map the 3-D refractivity into the slant path delay along the line-of-sight between the Envisat satellite and the ground:

$$\Delta L = 10^{-6} \int_{z}^{z_{satellite}} N(s)ds, \tag{1}$$

where s is the slant path, ΔL is the excess path delay, and z is the elevation. We ignore refractive bending because the incidence angles are small enough that this is insignificant. The refractivity N is given by

$$N = k_1\left(\frac{P_a Z_a^{-1}}{T}\right) + \left(k_2 + \frac{k_3}{T}\right)\frac{eZ_w^{-1}}{T}, \tag{2}$$

where the constants $k_1 = 0.776\,\mathrm{K\,Pa^{-1}}$, $k_2 = 0.716\,\mathrm{K\,Pa^{-1}}$, and $k_3 = 3.75 \times 10^3\,\mathrm{K^2\,Pa^{-1}}$. T is the temperature in Kelvin, and P_a and e are the partial pressures of dry air and water vapor, respectively. Z_a^{-1} and Z_w^{-1} are the inverse compressibility factors for dry air and water vapor given by [*Owens*, 1967]

$$Z_a^{-1} = 1 + 57.9 \times 10^{-8}\left(1 + \frac{0.52}{T}\right)P_a - 9.4611 \times 10^{-4}\frac{tP_a}{T^2}, \tag{3}$$

and

$$Z_w^{-1} = 1 + 1650\frac{e}{T^3}\left(1 - 0.01317t + 1.75^{-4}t^2 + 1.44 \times 10^{-6}t^3\right). \tag{4}$$

where $t = T$ - 273.15.

[21] Our LAPS domain includes pressure levels up to ~16.5 km (100 mbar). The slant-path integration could terminate here for InSAR correction purposes, because this encompasses all the significant delay variations; however, to be able to validate the ray-traced values against other data, such as GPS-estimated delays, we need to continue the integration to higher elevations. We add additional levels defined by the standard atmosphere model [*NASA*, 1966] to provide information up to 100 km. A final small additional

term is required to take into account the last remaining atmosphere above this elevation. For this component, the pressure and temperature at 100 km are used to determine the equivalent zenith delay, which is scaled using the (isotropic) Niell Hydrostatic [*Niell*, 1996] mapping function to attempt to determine the equivalent line-of-sight adjustment. Comparison with the GPS zenith neutral delay (ZND) estimates (Table 1) indicates that the LAPS integrated delays match the GPS estimates with a mean difference of ~1 cm and a standard deviation of 1.4 cm. Slightly higher than the typical formal error for the GPS estimates [e.g., *Bevis et al.*, 1992], this is the level of agreement that would be expected. The statistics indicate that the GPS + MADIS version of the LAPS runs agrees slightly better with the GPS than the other two. Figure 3 illustrates this further by plotting the residuals of the GPS and LAPS total delays from a mean exponential fit to the elevation. The clustering along a linear trend confirms that they agree quite closely on the magnitudes of the perturbations from a horizontally isotropic atmosphere.

[22] The SAR data acquisition times for the three tracks we used for Mount St. Helens (Table 2) are at ~10 min before 06:00, ~5 min after 06:00, and at ~18:30 UTC. Because the timing is close to the standard 06:00 and 18:00 output times for the MM5 prediction fields, and we are interested here in exploring the first-order effects of incorporating additional observations into the weather model predictions, we do not attempt to tailor our analysis to the exact minute of the observation time. This also allows us to explore the impact of the timing for the weather model products on the effectiveness of the mitigation approach. Examining the GPS delay time series indicates that the mean absolute changes in delay from the actual SAR observation time to the synoptic observation hour we use here are only 0.4, 0.8, and 1.3 mm, respectively, confirming that the bulk atmosphere is not changing significantly over these timescales.

[23] One of the more important additional data sets incorporated into the LAPS analysis stage is a higher-resolution digital elevation model (DEM) than is used in the coarse MM5 prediction. We use a smoothed, subsampled DEM based on the 1-arc sec Shuttle Radar Topography Mission (SRTM) DEM [*Farr et al.*, 2007]. Despite this significant improvement in the spatial resolution of the elevation model, as the LAPS output is on a 1-km grid, its surface height field is a smoothed version of the source DEM grid and so has slightly different values from the original DEM for any given point. To take this into account, while avoiding extrapolation of the near-surface fields, which often exhibit unrepresentatively strong gradients, we use an approach similar to the "stretched boundary layer model" [*Löfgren et al.*, 2010]. Specifically, we extend/contract the "free" atmosphere column, estimated from LAPS model levels several hundred meters above the nominal ground level, to adjust the LAPS modeled surface fields to their correct elevations.

Table 1. Differences Between Total Zenith Delays (cm) Estimated by the GPS Sites and From the LAPS Analyses at Those Locations

	MADIS	MADIS + GPS	MADIS + GPS + GOES
Mean (SD), cm	1.05 (1.43)	1.00 (1.38)	1.05 (1.39)

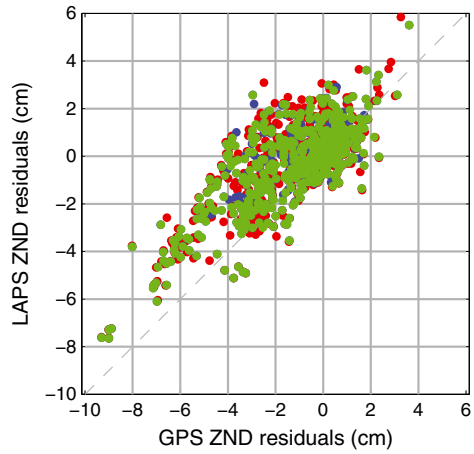

Figure 3. Scatter plot showing comparison between residuals for GPS estimated delays from a mean horizontally isotropic atmosphere with exponentially decaying delay with height and integrated delays from the three LAPS analyses (red, MADIS; green, GPS + MADIS; blue, GOES + GPS + MADIS).

[24] Because the LAPS DEM remains reasonably high-resolution and the elevation corrections are therefore relatively small (in fact, the corrections are almost constant over the conditions represented by our suite of interferograms), we find no significant differences between synthetic interferograms formed using the elevation-corrected or uncorrected ray-traced delay fields. We conclude that, for most conditions, discrepancies between the smoothed DEM applied by LAPS and the unsmoothed version do not introduce significant errors as long as the decimation is not too extreme.

5. InSAR Data

[25] We use a data set of 25 SAR scenes from the EarthScope and WInSAR archives for which MM5 predictions were available. The scenes cover the time period from June 2004 to August 2007 from three different look angles (Figure 2) and we formed 39 interferograms with which to test our approach. We used the two-pass method to generate interferograms [*Massonnet and Feigl*, 1998], removing the topographic contribution to phase using a hole-free, merged DEM based on the 1-arc sec SRTM data [*Farr et al.*, 2007] and U.S. Geological Survey national elevation data set DEM [*Gesch*, 1994]. To minimize orbital errors, interferogram baselines are calculated based on Envisat DORIS precise orbit state vectors.

6. Volcano Deformation

[26] Mount St. Helens experienced deflation during the period from 2004 to 2006. Although we are focused here on the atmospheric impact in InSAR images, it is important to compare the magnitudes of these artifacts with the ground motion signals and perform our statistical analyses of the effectiveness of our approach having separated variable refractivity effects from the effects of ground motion. Based on previous analyses of the deformation during this period

Table 2. InSAR Database Information for the Three Tracks Used and Percentage rms Reduction for Each LAPS-Corrected Interferogram With Respect to the rms of the Uncorrected Image

Track	Incidence Angle/ Image Swath	Heading (Ascending/Descending)	Acquisition Time (UTC/PST)	MADIS (Mean/Median), %	MADIS + GPS (Mean/Median), %	MADIS + GPS + GOES (Mean/Median), %
020	41 (IS6)	-10 (A)	06:04/22:04	102.0/101.7	101.5/100.2	101.6/100.2
156	23 (IS2)	-167 (D)	18:30/10:30	102.6/89.4	101.2/88.9	102.9/89.0
163	23 (IS2)	-13 (A)	05:50/21:50	93.4/95.0	91.8/92.5	99.8/93.2
All				98.6/94.7	97.5/92.6	101.2/93.4

[*Lisowski et al*., 2008], we model the predicted ground motion field using a vertical prolate ellipsoid to represent the magma chamber beneath the volcano and vary the depth of the chamber to approximately model the effects of variable topography. Changes in pressure within the ellipsoid over time are estimated from parameters determined by *Lisowski et al*. [2008]. The maximum line-of-sight deformation for the time intervals matching the interferogram are on the order of 2 cm—considerably smaller than the typical 5 cm amplitudes of residual signals (presumably due to atmospheric artifacts) in interferograms, and we conclude that, although Mount St. Helens was actively deforming during much of the time period of our study, these ground motions are not visible in the interferograms. We remove the modeled deformation from the interferograms before performing our statistical analyses and consider that any residual unmodeled motions do not introduce significant errors into our analysis.

7. Results

7.1. Direct Correction

[27] Direct subtraction of synthetic interferograms from actual interferograms worked quite well in some cases, but less so in most instances, and was occasionally counterproductive (Figure 4). A date pair for which LAPS predicts simple, height-dependent relative delay (Figure 4a–c) matches the observed interferogram very well, reducing a large part of the signal, except for a small residual on the southern rim of the volcano's summit. Despite this, the relatively small amplitude (<1 cm) ground signal predicted by the deformation model is still not evident. An example of a more typical case is shown in the bottom row in Figure 4d–f. Here, the LAPS analysis shows an increase in range in the northwest half of the image and a range decrease in the southeast half. Although the increased range matches well with the observed interferogram, the decrease does not,

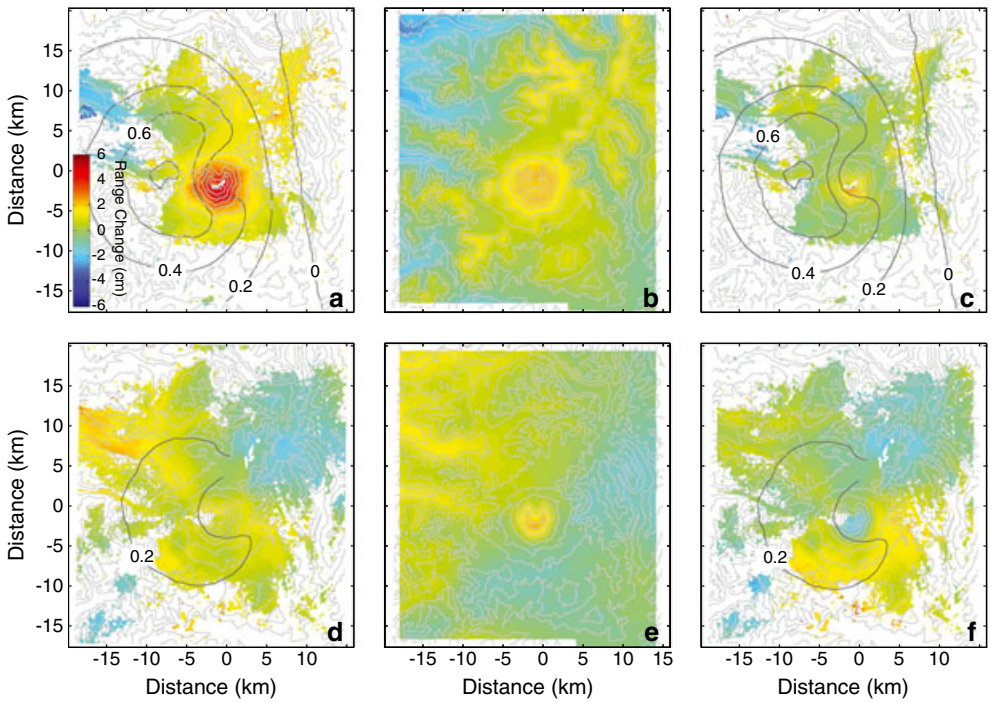

Figure 4. Examples of the performance of the atmospheric correction screens generated from the LAPS analyses using the best-performing GPS + MADIS assimilation. Columns show the interferogram, the LAPS-derived synthetic interferogram, and the LAPS-corrected interferogram from left to right. Predicted line-of-sight range change from the deformation model is shown in gray contours. Top row (a–c) presents an example of one of the best matches, for 13 July 2005 to 28 June 2006, showing a significant reduction in the interferogram signal. Bottom (d–f) row shows an example of a more typical case, for 14 May 2005 to 23 July 2005 where signal reductions in some quadrants of the interferogram are matched by increases in others. (Plots for all interferograms are included in the Supplementary Material.)

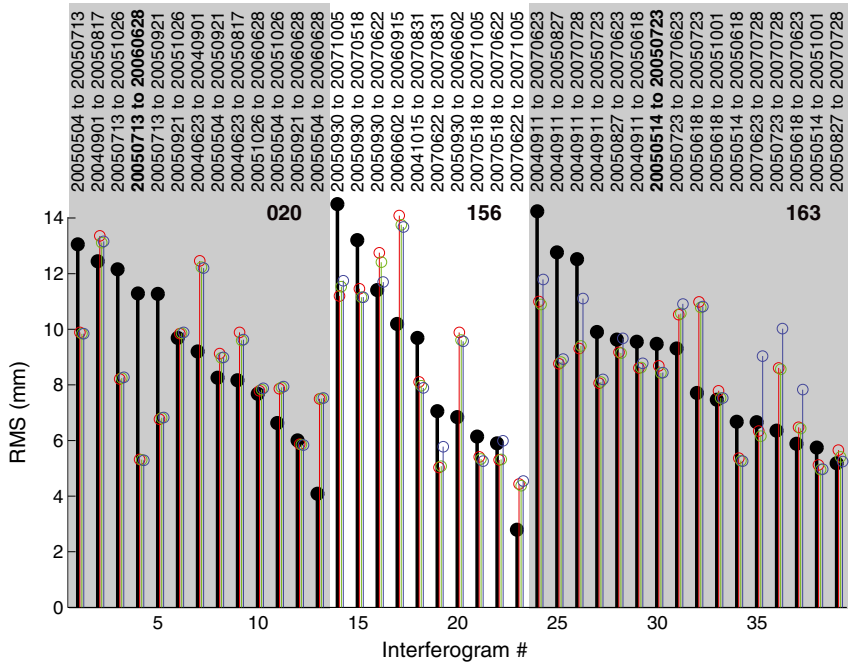

Figure 5. Stem plot showing the change in variance from the original interferograms (black) as corrections based on the LAPS analyses with MADIS (red), GPS + MADIS (green), and GPS + MADIS + GOES (blue) are subtracted. Interferograms are organized by track (Table 2) and then by uncorrected rms. Dates for the interferograms presented in Figure 4 are highlighted in bold.

with the net effect being that the noise in the northwest is reduced but increased equivalently in the southeast. In addition, the LAPS analysis generates a strong anomaly over the summit of Mount St. Helens, which is not seen in the InSAR data, producing a pronounced apparent range decrease in that location after correction. As before, the small predicted ground motion signal is not distinguishable from the noise. Using the rms as a measure of the noise in the interferogram, the overall benefits are modest (Figure 5; Table 2) at best, with only 5.3%, 7.5%, and 6.6% overall reduction of the median rms for the three different LAPS runs, respectively. As the mean rms shows no significant improvement from the corrections, the slight improvement indicated by the median suggests that modest improvements in a number of interferograms are being balanced by a few interferograms that are strongly negatively impacted. The LAPS run that included only the MADIS and GPS-derived delays unexpectedly performed the best of the three, suggesting that the introduction of the GOES products worsens the performance. It seems probable that the coarse, 4-km resolution of the GOES data generates "blocky" products that are inappropriate for use over small spatial windows. There is no obvious correlation between the proximity of the nominal weather model output time to the actual SAR acquisition times (Figure 5; Table 2), suggesting that time offsets up to ~30 min do not significantly impact the first-order effectiveness of this technique. The track with the least successful mitigation results is 020, acquired using image swath 6. This was the track with acquisition time closest to the nominal LAPS output time, so the poor performance must be related to the higher incidence angle. It is clear from Figure 5 that, in many interferograms, the mitigation has reduced atmospheric noise, but, percentage-wise, the lack of overall improvement suggests that higher incidence angle interferograms are harder to correct.

7.2. Statistical Comparison

[28] As the rms measure does not take into account the spatial coherence of the observed and predicted residuals, we now examine whether the LAPS models reproduce the spectral character recorded in the interferograms as a function of spatial wavelength. For interferograms shown in Figure 4, their respective variograms (Figure 6) illustrate the broad patterns revealed by the analysis. For the case where a significant improvement is found (Figure 6a), the variogram shows that the correction had no effect on the shorter wavelengths but was successful at reproducing the relative delays for wavelengths greater than 8 km, with up to two orders of magnitude reduction in variance for the longest (64 km) component. The more typical result is shown in Figure 6b: the LAPS analyses generate synthetic interferograms with approximately the same variances at most wavelengths, but the corrected interferogram shows no reduction in variance and actually has increased variance for the wavelengths shorter than 5 km. This suggests that, although the weather model is doing a good job of reproducing the general statistical state of the atmosphere at each time, it is putting the water vapor perturbations in the wrong locations. The anomalies in the original interferogram therefore go largely uncorrected, whereas new anomalies predicted by the LAPS models are added during the correction step. The variograms indicate that all three LAPS runs have virtually identical statistical distributions, reinforcing the conclusion that the additional data sets had little effect on the analyses. All the variograms, especially for the shorter wavelengths, follow the 5/3 slope predicted for 2-D

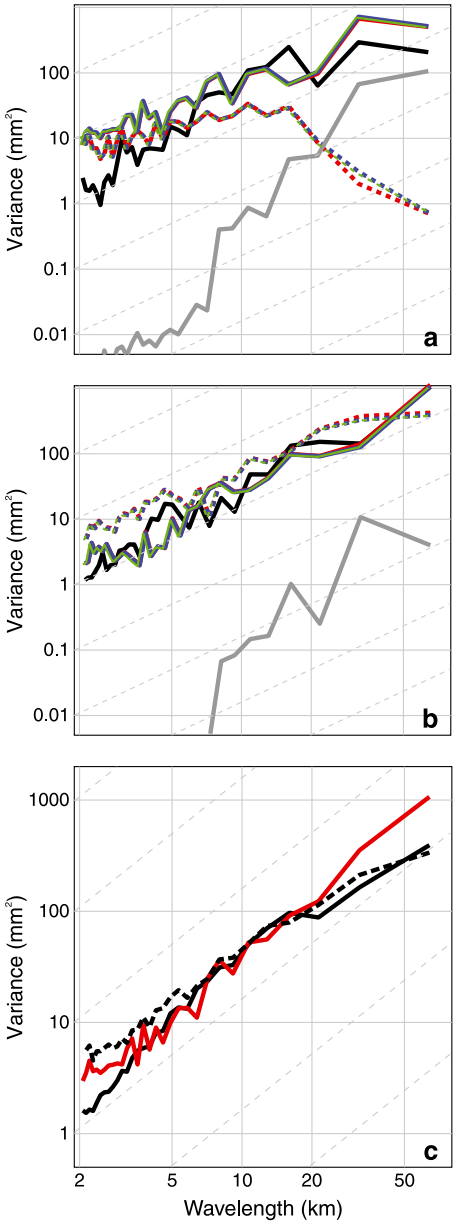

Figure 6. Variance versus spatial wavelength. (a and b) Two cases presented in Figure 4, with predicted volcanic deformation (gray), observed InSAR range change (black), line-of-sight range changes estimated from LAPS assimilations with MADIS (red), GPS + MADIS (green), and GPS + MADIS + GOES (blue), and the corrected interferograms (dashed red, green, and blue lines). (c) Mean variance for all date pairs showing original interferograms (solid black), GPS + MADIS LAPS analyses (red, the other analyses are indistinguishable), and corrected interferograms (dashed black). To detect the deformation, the corrected curves must drop below the deformation curve. Dashed lines indicate 5/3 slope expected for a turbulent medium.

maps of signals traveling through a 3-D turbulent medium [*Tatarskii*, 1961; *Treuhaft and Lanyi*, 1987; *Ruf and Beus*, 1997]. Figure 6 also shows the variograms for the predicted line-of-sight deformation. In general, these confirm that the power of the deformation signal is well below the power of the atmospheric noise, although, in the case of Figure 6a, the variance in the corrected interferogram is reduced enough for the longer wavelengths that the deformation could now be theoretically detectable.

[29] Figure 6c shows the mean variogram for all interferograms and the GPS + MADIS LAPS-based synthetic interferograms (the other LAPS versions are virtually indistinguishable), confirming that LAPS analyses reproduce the variance at almost all the wavelengths, although, interestingly, they show excess variance at the longest and shortest wavelengths. For the longer wavelengths, the downward step in power for the original interferograms suggests that some portion of the expected power may be absorbed into some other parameter(s) during the processing, overflattening the final interferograms. The limited spatial coherence of many scenes and the error this introduces into estimates of the spectral power may also contribute. At the shortest wavelengths, the LAPS variogram plots higher than that of the InSAR. As the interferogram's variogram extends the expected linear power-law trend, it seems the most plausibly correct, and it appears that the LAPS analyses are producing too much power below the original 4-km grid spacing. It is unclear why this might be occurring. We speculate that, due to the 4-km spacing of the MM5 prediction fields used as background, the LAPS analyses are unable to properly represent important processes operating at shorter wavelengths and "aliasing" may be occurring.

7.3. Predictability of Atmospheric Analysis Performance

[30] Although we find that, overall, the effect of the corrections based on the analyses is insignificant, it is also true that, in some cases, the corrections do a good job of reducing the noise (e.g., Figure 4a–c). The corrections could therefore still be of significant value if it were possible to independently determine which model outputs will help (rather than hinder) the correction process. Other studies have noted that models do well at matching the average isotropic vertical structure and less well at tracking spatial heterogeneities [*Hanssen*, 2001]. To test whether analyses describing a largely horizontally isotropic atmosphere perform better at correcting the interferograms, we form a predictive measure by calculating the residual LAPS delays from a simple best-fit, elevation-dependent exponential function:

$$ZND_{res}(x,y) = ZND(x,y) - ZND_0 e^{-bz}. \quad (5)$$

[31] Here, ZND is the zenith neutral delay, ZND_0 and b are constants estimated from the elevation-dependent fit, and ZND_{res} is the residual after removing the modeled fit from the observed values. In general, the exponential fit is a good description of the delay profiles and has only small residuals. We would expect a correlation between high rms values of these residuals and rms measures of the scatter in the original and corrected SAR data if poor performance is related to strong nonvertical variations from a simple elevation-dependent behavior. As is clear from Figure 7, this does not seem to be the case. Similarly, there is no correlation between the percentage reduction in rms due to the correction and the rms of the residuals (Figure 7c).

[32] A related, but slightly different, hypothesis connects poor performance to a highly dynamic atmosphere due to,

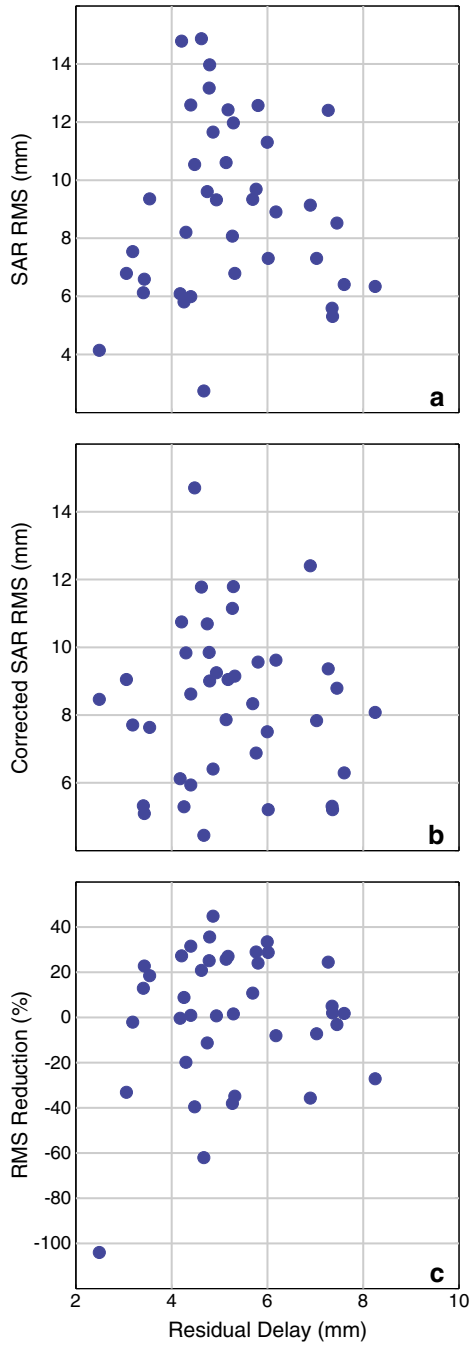

Figure 7. Scatter plot showing relationship between the rms of the residuals from a simple exponential function of height for the 39 synthetic LAPS (using GPS + MADIS) interferograms and (a) original InSAR rms, (b) rms for InSAR corrected using GPS + MADIS LAPS analysis, and (c) percentage reduction in mean rms with correction step.

for example, strongly convective conditions or a strong wind field. It seems plausible that these conditions would be the most difficult for the weather models to reproduce in detail. We test this hypothesis using two predictors. The lifted index (LI) is commonly used as a meteorological indicator of the vertical stability of the atmosphere. Negative values indicate increasingly unstable conditions prone to deep convection and thunderstorm activity. To form a measure for the

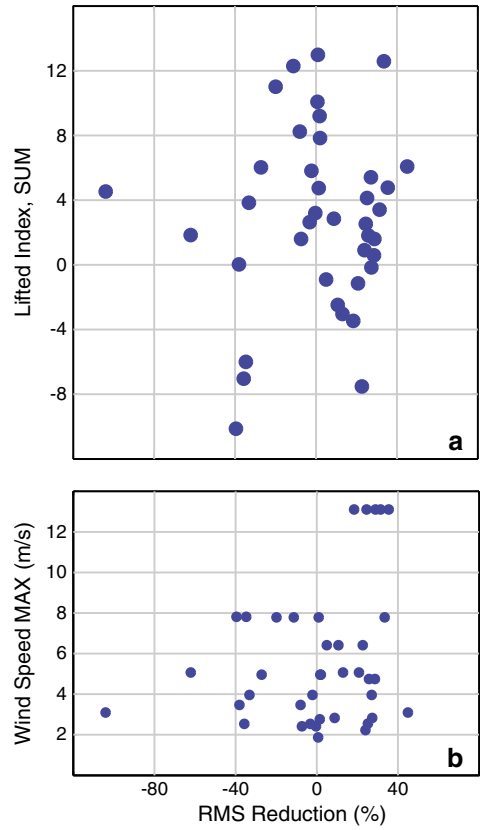

Figure 8. Scatter plot showing relationship between percentage change (from 100%) in mean rms and (a) sum of the LI for each pair and (b) the maximum wind speed for each pair.

date pair in each interferogram, we find the minimum LI for the area around Mount St. Helens for each date and take the sum of values for the two dates. If strongly convective atmospheres are the cause of poor performance of our technique, we would expect to see a correlation between our LI measure and performance. Again, however, we find no correlation (Figure 8a). Similarly, choosing the mean wind speed at 850 mbar in the vicinity of Mount St. Helens as representative of windy local conditions still results in no correlated rms reduction (Figure 8b).

8. Conclusions

[33] NWMs can provide analyses describing the state of the atmosphere explicitly at the time of satellite SAR acquisitions. Adding an extra stage after the production of a NWM prediction, where all contemporaneous meteorological data are assimilated along with the predicted state of the atmosphere to generate an analysis of the state of the atmosphere at that time, should provide a more accurate estimate of atmospheric conditions and could be a powerful method for incorporating all available data. For this to be effective, however, the initial predicted fields need to be a reasonable approximation to the actual state, and the additional data to be ingested should be sufficient to allow the assimilation routines to perturb the fields into an even more accurate description of the real state of the atmosphere. If either the initial field is relatively poor or the quantity and

quality of additional data is insufficient (or both), even the addition of this final assimilative step will be ineffective at generating a sufficiently accurate description of the atmosphere that is useful for our extremely demanding application. In the case we examine here, of InSAR data from Mount St. Helens during 2004–2007, there is little overall mean improvement, although more interferograms are improved than degraded. Assimilating local GPS-derived delay/precipitable water produces the best model performance, whereas higher incidence angles appear to reduce the effectiveness of the approach. The exact timing of the simulation is not a major issue in our experiments.

[34] We are unable to find any simple indicator based on the SAR or LAPS data sets, which predicts whether the atmospheric phase screen correction will improve or degrade an interferogram. Without some reliable predictor of performance, even the selective use of the NWM analyses for a limited subset of scenes becomes problematic. This suggests that, for areas with complex meteorology and relatively sparse observations, efforts based on NWM predictions and analyses of the delay at a specific time may not be productive. Despite this negative result, some broader statistics of the predicted atmospheric delay match those from the interferograms. This information is potentially useful, for example, as a weighting function during stacking or for guiding the design of filters applied in time-series analysis. For areas without significant local meteorological observing capacity such as the one studied here, however, this information could be determined as effectively from regional weather prediction fields, without the need to establish and operate a dedicated local analysis.

[35] Our experience indicates that considerably more meteorological data are required to constrain both the initial weather model prediction and the final assimilation than was available for Mount St. Helens. It is possible, therefore, that the weather model approach is currently only viable where the atmosphere is less dynamic and thus more predictable such as in continental interiors, at high elevations, or during periods with low water vapor concentration and variability, or for locations with an extensive meteorological observation network. The area around Los Angeles, California, has a dense and extensive GPS network that can provide these data and would be an interesting test of this hypothesis. Indeed, correction phase screens based purely on GPS data have proven effective at reducing atmospheric noise for this area [*Löfgren et al*., 2010]. Assimilating those GPS delay solutions into a NWM package such as LAPS should provide a further improvement by applying appropriate physics to properly interpolate and extrapolate the new information across gaps in the observational network.

[36] Alternative advanced approaches such as 4-D VAR [e.g., *Rabier et al*., 2000] offer interesting and powerful opportunities to apply NWM technologies to the problem of atmospheric mitigation for InSAR. These models operate by ingesting all new observations at each time step, adjusting both the current and the previous states of the atmosphere to properly accommodate the new observations. This approach should extract the maximum information from limited observations and could be ideal for InSAR applications, although the setup and computational effort to run these models is large. Finally, we note that not only do NWM packages continue to evolve and computational processing power increases, but also meteorological observational capacity is similarly expanding. As a consequence, it seems likely that the approach we find in this study to be inadequate may prove increasingly viable in the near future, and we therefore recommend continued experimentation with NWM techniques for atmospheric mitigation.

[37] **Acknowledgments.** This work was supported by National Science Foundation under Grant No. 0746394 and used data provided by the Plate Boundary Observatory operated by UNAVCO for EarthScope (www.earthscope.org) and supported by the National Science Foundation (No. EAR-0350028 and EAR-0732947). Reviews by G. Wadge, M. Poland, S. Jónsson, and an anonymous reviewer improved the article.

References

Albers, S. C., J. A. McGinley, D. L. Birkenheuer, and J. R. Smart (1996), The Local Analysis and Prediction System (LAPS): Analyses of clouds, precipitation, and temperature, *Wea. Forecast.*, *11*(3), 273–287, doi: 10.1175/1520-0434(1996)011<0273:tlaaps>2.0.co;2.

Barnes, S. L. (1964), A technique for maximizing details in numerical weather map analysis, *J. Appl. Meteor.*, *3*(4), 396–409.

Berardino, P., G. Fornaro, R. Lanari, and E. Sansosti (2002), A new algorithm for surface deformation monitoring based on small baseline differential SAR interferograms, *Geosci. Remote Sens., IEEE Transact. on*, *40*(11), 2375, doi: 10.1109/TGRS.2002.803792.

Bevis, M., S. Businger, T. A. Herring, C. Rocken, R. A. Anthes, and R. H. Ware (1992), GPS Meteorology: Remote sensing of atmospheric water vapor using the global positioning system, *J. Geophys. Res.*, *97*, 15,787–715,801.

Burgmann, R., D. Schmidt, R. M. Nadeau, M. d'Alessio, E. Fielding, D. Manaker, T. V. McEvilly, and M. H. Murray (2000), Earthquake potential along the northern Hayward Fault, California, *Science*, *289*(5482), 1178–1182.

Businger, S., R. McClaren, R. Ogasawara, D. Simons, and R. J. Wainscoat (2001), Starcasting, *Bull. Am. Meteor. Soc.*, *83*(6), 858–871.

Cherubini, T., S. Businger, C. Velden, and R. Ogasawara (2006), The impact of satellite-derived atmospheric motion vectors on mesoscale forecasts over Hawaii*, *Mon. Wea. Rev.*, *134*(7), 2009–2020, doi: 10.1175/mwr3163.1.

Doin, M. P., C. Lasserre, G. Peltzer, O. Cavalié, and C. Doubre (2009), Corrections of stratified tropospheric delays in SAR interferometry: Validation with global atmospheric models, *J. Appl. Geophys.*, *69*(1), 35–50, doi: 10.1016/j.jappgeo.2009.03.010.

Eff-Darwich, A., J. Pérez, J. Fernández, B. García-Lorenzo, A. González, and P. González (2012), Using a mesoscale meteorological model to reduce the effect of tropospheric water vapour from DInSAR data: A case study for the island of Tenerife, Canary Islands, *Pure Appl. Geophys.*, *169*(8), 1425–1441, doi: 10.1007/s00024-011-0401-4.

Elliott, J. R., J. Biggs, B. Parsons, and T. J. Wright (2008), InSAR slip rate determination on the Altyn Tagh Fault, northern Tibet, in the presence of topographically correlated atmospheric delays, *Geophys. Res. Lett.*, *35*(12), L12309, doi: 10.1029/2008gl033659.

Emardson, T. R., M. Simons, and F. H. Webb (2003), Neutral atmospheric delay in interferometric synthetic aperture radar applications: Statistical description and mitigation, *J. Geophys. Res.*, *108*(B5), 2231–2238, doi: 10.1029/2002JB001781.

Farr, T. G., et al. (2007), The Shuttle Radar Topography Mission, *Rev. Geophys.*, *45*(2), RG2004, doi: 10.1029/2005rg000183.

Ferretti, A., C. Prati, and F. Rocca (2001), Permanent Scatterers in SAR Interferometry, *IEEE Trans. Geosci. Remote Sens.*, *39*(1), 8–20.

Fialko, Y., M. Simons, and D. Agnew (2001), The complete (3-D) surface displacement field in the epicentral area of the 1999 Mw7.1 Hector Mine earthquake, California, from space geodetic observations, *Geophys. Res. Lett.*, *28*, 3063–3066.

Foster, J., B. Brooks, T. Cherubini, C. Shacat, S. Businger, and C. L. Werner (2006), Mitigating atmospheric noise for InSAR using a high resolution weather model, *Geophys. Res. Lett.*, *33*, L16304, doi: 10.1029/2006GL026781.

Garand, L. (1983), Some improvements and complements to the infrared emissivity algorithm Including a parameterization of the absorption in the continuum region, *J. Atmos. Sci.*, *40*(1), 230–243, doi: 10.1175/1520-0469(1983)040<0230:siactt>2.0.co;2.

Gesch, D. B. (1994), Topographic Data Requirements for EOS Global Change Research *Open-File Report 94-626*, 66p pp, U. S. Geological Survey.

Grell, G. A., J. Dudhia, and P. J. Stauffer (1995), A Description of the Fifth-Generation Penn State / NCAR Mesoscale Model (MM/5), 122 pp, NCAR / TN-398 + STR, Boulder, Co.

Hanssen, R. F. (1998), *Atmospheric heterogeneities in ERS tandem SAR interferometry DEOS Report No. 98.1*, 136 pp, Delft University Press, Delft.

Hanssen, R. F. (2001), *Radar interferometry: data interpretation and error analysis*, Kluwer Academic Publishers, Dordrecht, The Netherlands.

Hanssen, R. F., T. M. Weckwerth, H. A. Zebker, and R. Klees (1999), High-resolution water vapor mapping from interferometric radar measurements, *Science*, *283*(5406), 1297–1299, doi: 10.1126/science.283.5406.1297.

Herring, T. A., R. W. King, and S. McClusky (2006), GAMIT Reference Manual, GPS Analysis at MIT, Release 10.3, Massachussetts Institute of Technology, Cambridge.

Hiemstra, C. A., G. E. Liston, R. A. Pielke, D. L. Birkenheuer, and S. C. Albers (2006), Comparing Local Analysis and Prediction System (LAPS) assimilations with independent observations, *Wea. Forecast.*, *21*(6), 1024–1040, doi: 10.1175/waf961.1.

Hooper, A., H. Zebker, P. Segall, and B. Kampes (2004), A new method for measuring deformation on volcanoes and other natural terrains using InSAR persistent scatterers, *Geophys. Res. Lett.*, *31*, 5, doi: 10.1029/2004GL021737.

Jolivet, R., R. Grandin, C. Lasserre, M. P. Doin, and G. Peltzer (2011), Systematic InSAR tropospheric phase delay corrections from global meteorological reanalysis data, *Geophys. Res. Lett.*, *38*(17), L17311, doi: 10.1029/2011gl048757.

Jónsson, S., H. Zebker, P. Segall, and F. Amelung (2002), Fault slip distribution of the 1999 Mw 7.1 Hector Mine, California, earthquake, estimated from satellite radar and GPS measurements, *Bull. Seismol. Soc. Am.*, *92*(4), 1377–1389, doi: 10.1785/0120000922.

Kain, J. S., and J. M. Fritsch (1990), A one-dimensional entraining/detraining plume model and its application in convective parameterization, *J. Atmos. Sci.*, *47*(23), 2784–2802, doi: 10.1175/1520-0469(1990)047<2784:aodepm>2.0.co;2.

Li, Z., J.-P. Muller, P. Cross, and E. J. Fielding (2005), Interferometric Synthetic Aperture Radar (InSAR) atmospheric correction: GPS, Moderate Resolution Imaging Spectroradiometer (MODIS), and InSAR integration, *J. Geophys. Res.*, *110*(B03410), doi: 10.1029/2004JB003446.

Li, Z., J.-P. Muller, P. Cross, P. Albert, J. Fischer, and R. Bennartz (2006), Assessment of the potential of MERIS near-infrared water vapour products to correct ASAR interferometric measurements, *Int. J. Remote Sens.*, *27*(1-2), 349–365, doi: 10.1080/01431160500307342.

Lisowski, M., D. Dzurisin, R. P. Denlinger, and E. Y. Iwatsubo (2008), GPS-measured deformation associated with the 2004–2006 dome-building eruption of Mount St. Helens, Washington, in *A Volcano Rekindled: The Renewed Eruption of Mount St. Helens, 2004-2006*, edited by D. R. Sherrod, W. E. Scott, and P. H. Stauffer, pp. 301–333, U.S. Geological Survey, Reston, Virginia.

Löfgren, J. S., F. Björndahl, A. W. Moore, F. H. Webb, E. J. Fielding, and E. F. Fishbein (2010), Tropospheric correction for InSAR using interpolated ECMWF data and GPS Zenith Total Delay from the Southern California Integrated GPS Network, paper presented at Geoscience and Remote Sensing Symposium (IGARSS), 2010 IEEE International, 25-30 July 2010.

Massonnet, D., and K. L. Feigl (1998), Radar interferometry and its application to changes in the earth's surface, *Rev. Geophys.*, *36*(4), 441–500.

Massonnet, D., M. Rossi, C. Carmona, F. Adragna, G. Peltzer, K. Feigl, and T. Rabaute (1993), The displacement field of the Landers earthquake mapped by radar interferometry, *Nature*, *364*(6433), 138–142.

McGinley, J. A. (1989), The Local Analysis and Prediction System, in *Preprints, 12th Conf. on Analysis and Forecasting*, edited, pp. 15–20, Amer. Meteor. Soc., Monterey, CA.

McGinley, J. A., S. C. Albers, and P. A. Stamus (1991), Validation of a convective index as defined by a real-time local analysis system, *Wea. Forecast.*, *6*, 337–356.

NASA (1966), U.S. Standard Atmosphere Supplements, 1966, U.S. Committee on Extension to the Standard Atmosphere, U.S. Government Printing Office, Washington D.C.

Niell, A. E. (1996), Global mapping functions for the atmosphere delay at radio wavelengths, *J. Geophys. Res.*, *101*, 3227–3246.

Onn, F., and H. Zebker (2006), Correction for interferometric synthetic aperture radar atmospheric phase artifacts using time series of zenith wet delay observations from a GPS network, *J. Geophys. Res.*, *111*, B09102, doi: 10.1029/2005JB004012.

Owens, J. C. (1967), Optical refractive index of air: Dependence on pressure, temperature and composition, *Appl. Opt.*, *6*(1), 51–59.

Pinel, V., A. Hooper, S. De la Cruz-Reyna, G. Reyes-Davila, M. P. Doin, and P. Bascou (2011), The challenging retrieval of the displacement field from InSAR data for andesitic stratovolcanoes: Case study of Popocatepetl and Colima Volcano, Mexico, *J. Volcanol. Geotherm. Res.*, *200*, 49–61, doi: 10.1016/j.jvolgeores.2010.12.002.

Poland, M. P., and Z. Lu (2008), Radar Interferometry Observations of Surface Displacements during Pre- and Coeruptive Periods at Mount St. Helens, Washington, 1992-2005, in *A Volcano Rekindled: The Renewed Eruption of Mount St. Helens, 2004-2006*, edited by D. R. Sherrod, W. E. Scott, and P. H. Stauffer, pp. 361–382, U.S. Geological Survey, Reston, Virginia.

Puysségur, B., R. Michel, and J.-P. Avouac (2007), Tropospheric phase delay in interferometric synthetic aperture radar estimated from meteorological model and multispectral imagery, *J. Geophys. Res.*, *112*, B05419, doi: 10.1029/2006JB004352.

Rabier, F., H. Järvinen, E. Klinker, J.-F. Mahfouf, and A. Simmons (2000), The ECMWF operational implementation of four dimensional variational assimilation. Part I: Experimental results with simplified physics, *Q. J. R. Meteorol. Soc.*, *126*, 1143–1170.

Reisner, J., R. M. Rasmussen, and R. T. Bruintjes (1998), Explicit forecasting of supercooled liquid water in winter storms using the MM5 mesoscale model, *Q. J. R. Meteorol. Soc.*, *124*(548), 1071–1107, doi: 10.1002/qj.49712454804.

Ruf, C. S., and S. E. Beus (1997), Retrieval of tropospheric water vapor scale height from horizontal turbulence structure, *Geosci. Remote Sens., IEEE Transac. on*, *35*(2), 203–211, doi: 10.1109/36.563258.

Sandwell, D. T., L. Sichoix, D. Agnew, Y. Bock, and J.-B. Minster (2000), Near real-time radar interferometry of the Mw 7.1 Hector Mine earthquake, *Geophys. Res. Lett.*, *27*(19), 3101–3104.

Shaw, J. H., and P. M. Shearer (1999), An Elusive Blind-Thrust Fault Beneath Metropolitan Los Angeles, *Science*, *283*(5407), 1516–1518.

Skamarock, W. C., J. B. Klemp, J. Dudhia, D. O. Gill, M. Barker, W. Wang, and J. G. Powers (2005), A description of the Advanced Research WRF Version 2, 100 pp, NCAR Tech Notes-468 + STR, Boulder, CO.

Stephens, G. L. (1978), Radiation Profiles in Extended Water Clouds. II: Parameterization Schemes, *J. Atmos. Sci.*, *35*(11), 2123–2132, doi: 10.1175/1520-0469(1978)035<2123:rpiewc>2.0.co;2.

Tatarskii, V. I. (1961), *Wave propagation in a turbulent medium*, 285 pp., McGraw-Hill, New York.

Treuhaft, R. N., and G. E. Lanyi (1987), The effect of the dynamic wet troposphere on radio interferometric measurements, *Radio Sci.*, *22*, 251–265.

Troen, I. B., and L. Mahrt (1986), A simple model of the atmospheric boundary layer; sensitivity to surface evaporation, *Boundary-Layer Meteorol.*, *37*(1), 129–148, doi: 10.1007/bf00122760.

Wadge, G., et al. (2002), Atmospheric models, GPS and InSAR measurements of the tropospheric water vapour field over Mount Etna, *Geophys. Res. Lett.*, *29*(19), 1905, doi: 10.1029/2002GL015159.

Walls, C., T. Rockwell, K. Muellers, Y. Bock, S. Williams, J. Pfanner, J. Dolan, and P. Fang (1998), Escape tectonics in the Los Angeles metropolitan region and implications for seismic risk, *Nature*, *394*, 356–360.

Webley, P. W., G. Wadge, and I. N. James (2004), Determining radio wave delay by non-hydrostatic atmospheric modelling of water vapour over mountains, *Phys. Chem. Earth*, *29*(2-3), 139, doi: 10.1016/j.pce.2004.01.013.

Webley, P. W., R. M. Bingley, A. H. Dodson, G. Wadge, S. J. Waugh, and I. N. James (2002), Atmospheric water vapour correction to InSAR surface motion measurements on mountains: results from a dense GPS network on Mount Etna, *Phys. Chem. Earth*, *27*(4-5), 363–370, doi: 10.1016/S1474-7065(02)00013-X.

Zebker, H. A., P. A. Rosen, and S. Hensley (1997), Atmospheric effects in interferometric synthetic aperture radar surface deformation and topographic maps, *J. Geophys. Res.*, *102*(B4), 7547–7563.